Wind Turbine Tip Vortices under the influence of Wind Tunnel Blockage Effects

Wind Turbine Tip Vortices under the influence of Wind Tunnel Blockage Effects

R. Soto-Valle[1], J. Alber[1], M. Manolesos[2], C. N. Nayeri[1] and C. O. Paschereit[1]

[1] Technische Universität Berlin, Hermann-Föttinger Institut, Müller-Breslau-Straße 8, 10623 Berlin, Germany
[2] College of Engineering, Swansea University, Bay Campus, Fabian Way, Swansea, SA1 8EN, UK

E-mail: rodrigo.soto@campus.tu-berlin.de

Abstract. The current paper describes the characteristics of the tip vortex in the near wake of a three-bladed upwind horizontal axis wind turbine with a rotor diameter of 3 m. Phase-locked stereo particle image velocimetry measurements were carried out under the influence of the wind tunnel walls that create a high blockage ratio. The location of the vortex, convection velocity, core radius, and strength were investigated and compared with similar investigations, including different blockages cases. Additionally, the same performance of the wind turbine model was simulated in the open source wind turbine tool QBlade, using the lifting line free vortex wake module in the absence of the walls.

The results showed that the location of the tip vortices was more inboard the tip and more downstream the tunnel compared to the simulations and similar experiments. The convection velocity remained similar in the axial direction and changed in the lateral direction, contributing to the delay of the movement of the tip vortex outboard the tip. The strength, based on the circulation, was found with a difference of 4% between simulation and experiment.

1. Introduction

Wake effects and their interaction play a significant role in wind farm layout and performance. The wake of a single wind turbine is strongly affected by the shedding of the tip vortices (TVs). They are responsible for the complex flow field in the wake, producing strong gradients and instabilities [1]. For this reason, TVs have received significant attention within the wind energy research community.

N.J. Vermeer carried out several studies in the wake of a rotor model using a radial traverse equipped with hotwire probes that highlighted important conclusions for further research: The TV structure does not travel with the average velocity between inside and outside the wake, as was used under the assumption of roller bearing [2]. Instead, the TV exhibits a higher velocity [3] which remains constant in the axial direction. The TV strength depends on local conditions, rather than global and integrated quantities [4]. Its diameter decreases by expanding the wake while increases its diameter by aging [5].

New and less invasive techniques have been developed through the years, with particle image velocimetry (PIV) gaining popularity due to its non-intrusive nature and higher spatial resolution compared to anemometers or hot wire sensors. Some relevant investigations on wind turbine models are briefly described as follows.

The constant axial convection velocity was confirmed by the MEXICO project [6, 7] by means of the linear evolution of the axial location of the TV at tip speed ratios (TSR) of 4.2 and 6.7. However, when the TSR increases up to 10, the wake expansion becomes stronger and the velocity changes.

Maalouf et al. [8] showed that the TV expands in the radial direction, therefore the flow tube diameter increases. In addition, the concept of unsteadiness of the TV location was analyzed. The concept is known as jittering [8] or wandering [9] and is related to TV aging, turbulence in the tunnel, vibrations of the model turbine (e.g. blades and tower) and also the optic tools setup (PIV system). One option to eliminate this effect is using the conditional averaging [10].

Hu et al. [9] presented that the wandering of the TVs increases downstream the turbine and the probability density function of the TV location behaves like a normal distribution around the average vortex core position. Additionally, as the TSR increases, the gap between the helicoidal vortex tubes is reduced and the TV strength decreases.

Micallef et al. [11] used PIV measurements and a 3D unsteady potential-flow vortex model to show that once released, the TV vorticity rapidly becomes round and symmetrical. Another important remark is that the position of the TV core location starts inboard of the tip, in agreement with previous experiments of the TVs structure and location [12, 13].

Ostovan et al. [14] demonstrated that the TV swirl velocity can be reproduced by several laminar and turbulent models. In the same work, it was shown that the convection velocity, core size, and expansion increase with the implementation of winglets.

In the case of wind tunnel experiments with wind turbine models, the interaction between the model, its wake, and the walls of the wind tunnel is particularly complex [15]. Induction factor differences between a model considered in the absence of walls and wind tunnel experiments [6] demonstrate that tunnel effects and blockage influences are crucial.

This paper aims to characterize the effect of the wind tunnel walls on the TV. The focus will be on TV characteristics, such as position, radius, circulation, convection and swirl velocity. To achieve that, new measurement data were obtained from a stereoscopic particle image velocimetry (SPIV) system and compared with published experimental results from different wind turbine models and blockage ratios. Additionally, the experimental values were compared against the numerical result from the tool QBlade [16] and the TVs swirl velocity model developed by Vatistas [17].

The following sections show the experimental setup and methodology. The results and comparisons are presented in Sect. 4 followed by the conclusions in Sect. 5.

2. Experimental setup

The experiments were carried out in the close circuit wind tunnel at the Hermann-Föttinger Institut of the Technische Unversität Berlin (see Fig. 1). The research wind turbine was positioned in the large test section, with a cross-sectional area of $4.2 \times 4.2\ m^2$ and a length of $8\ m$. The freestream velocity was set to $u_\infty = 6.5\ ms^{-1}$ and the rotational speed to $f = 3\ Hz$, resulting in a tip speed ratio of $\lambda = 4.35$. The turbulence intensity reaches values up to $Ti = 6\%$, in contrast to the previous work [18, 19], which was attributed to the absence of the filtermat upstream the turbine.

The wind turbine model was the Berlin Research Turbine (BeRT) [20], which is a three-bladed, upwind horizontal axis wind turbine model with a rotor diameter of $D = 3\ m$ that creates a blockage ratio of $\beta_{BeRT} = 40\%$. Figure 2 shows the turbine inside the test section.

The blades were twisted, tapered, and use a Clark Y airfoil profile. From the radial position $r/R = 0.95$ the blade is tapered towards leading and trailing edge until the tip, passing from a chord length of 132 mm until the tip chord length of 12 mm. This design gives the tip a sword shape [21], as can be seen in Fig. 3. The Reynolds number was in the range of $Re = 23k - 257k$ based on the chord length aforementioned.

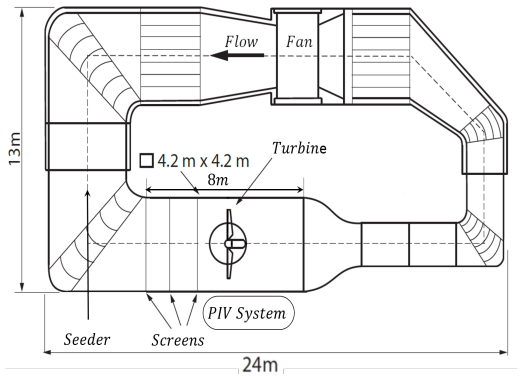

Figure 1. Wind tunnel sketch, test rig and PIV system positioning.

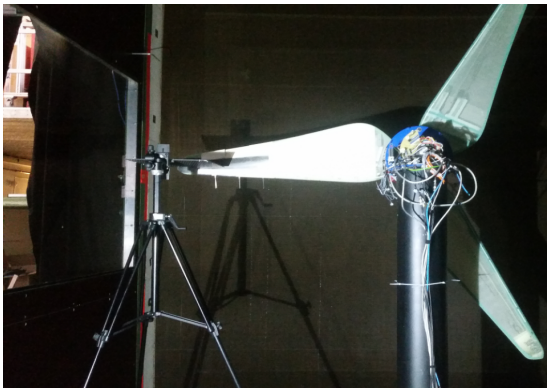

Figure 2. BeRT in the test section looking from downstream. Optical access on the left.

The velocities measurements were performed using a SPIV system (See Fig. 3). The measurement system consisted of a Quantel Dual-Nd:Yag Double Laser with energy of $171mJ$, a mirror arm, the laser sheet optics, two 14bit PCO 2000 cameras with a CCD-Chip resolution of 2048×2048 pixel, and an ILA synchronizer connected to the measurement computer. The reference blade position was obtained through a Hall effect sensor located in the nacelle and was used as a trigger of the PIV system.

The measurement plane was horizontal (X-Y plane, Fig. 4) and was centered at the tip location when the blade was at the horizontal position (see Fig. 3). The azimuth angle was defined at this position as $\phi = 0°$ so it coincides with the TV ages. Table 1 shows the image acquisition specifications for the measurement.

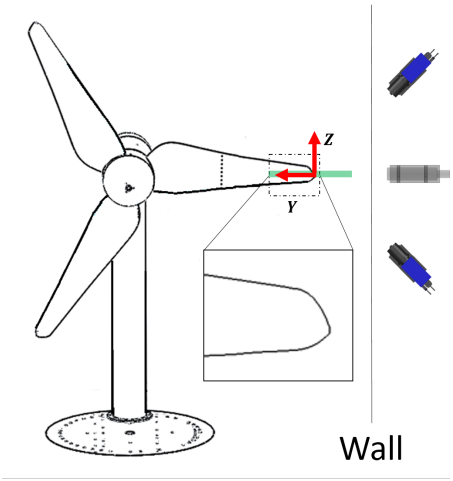

Figure 3. Details of PIV system position and tip blade shape, looking from upstream (not to scale).

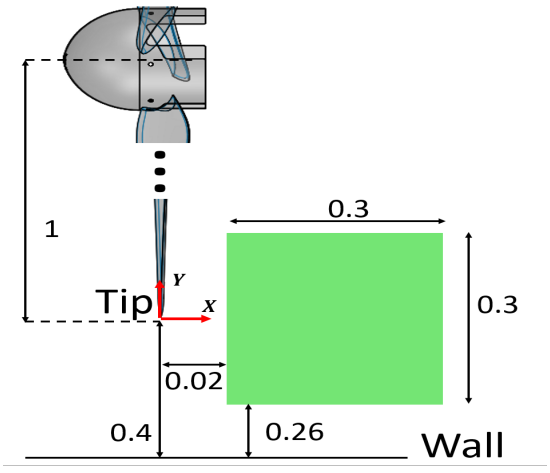

Figure 4. Field of view (top view). Dimensions normalized by the rotor radius (not to scale).

Phase-locked SPIV measurement over the rotor progression, i.e. vortex ages, were studied, in the azimuth range of $\phi = 35° - 60°$, incrementally with steps of $\Delta\phi = 5°$. The azimuth positions were chosen as the best compromise between reducing laser reflections from the blade and measuring the tip vortices as close to the tip as possible. One blade was set as a reference and synchronized with the laser and cameras to register the same azimuth position until a total of 1200 images pairs were recorded.

Table 1. Image acquisition specifications for the current case.

Item	
Cameras	PCO 2000
Lens focal length	100 mm
Resolution	2048×2048 px^2
Field of view	435×435 mm^2
Recordings	1200 images pairs
Laser pulse separation	150 μs
Interrogation window	24×24 px^2 (50% overlapping)
Spatial resolution	3.6 mm

3. Methodology

3.1. Particle image velocimetry procedure

The location of the TV center was defined as the location of the Q-criterion [22] maximum value. With all TV centers identified the method proposed by van der Wall [23] was applied, performing conditional average. The centers were shifted to coincide with each other to afterward interpolate and average all the data in a new grid. This allows eliminating the TV jittering. The resulting velocity fields permit to determinate the TV convection speed as the velocities in its center (u_c, v_c). The convection speed was subtracted from the respective velocity field, in order to obtain only the vortex-induced velocities.

The core radius, r_c, was estimated as the distance between the core center and the maximum swirl velocity position, $v_{\theta,max}$. In order to compare the results with the TV models, a swirl velocity distribution was chosen parallel to the y axis in the TV center line. The circulation was calculated by integrating the vorticity field over the vortex surface.

3.2. Numerical and analytical approaches

The examined cases were tested using the Vatistas TV model [17] as shown in Eq. 1. In the model, the normalized swirl velocity is a function of the normalized vortex radius, $\xi = r/r_c$. Subsequently, the turbulence parameter α was calculated by applying a fit using the measured velocities and Eq. 1.

$$\frac{v_\theta}{v_{\theta,max}} = \xi \left(\frac{\alpha + 1}{\alpha + \xi^4} \right)^m, \; m = \frac{\alpha + 1}{4}. \tag{1}$$

Additionally, the results were compared with the simulations of the open source wind turbine tool QBlade, using the lifting line free vortex wake module [24].

For the simulation, the blades were discretized in 28 equidistant panels, the inflow velocity was set as uniform and with the same magnitude of the wind tunnel experiment, $u_\infty = 6.5\ ms^{-1}$ and the rotation speed at $f = 3\ Hz$.

An azimuthal discretization of 5° was chosen and the simulation was performed until fully converged. The flow field was extracted at the same plane as the PIV measurements and at the same azimuth stations, i.e. $\phi = 35° - 60°$. More information can be found in the previous work of Marten et al. [25]. One important remark for the simulation is that the wind tunnel walls were not included. This allows making a comparison with a far-field condition.

3.3. Comparison with experimental literature

Several published research projects were compared with the current study. The selected experiments differ in blockage ratio, but all include PIV measurements of the TV. A summary of the experimental results to compare is shown in Table 2. The blockage was defined as the ratio between the rotor area (A_{model}) and the tunnel cross-sectional area in the test section (A_{tunnel}), $\beta = A_{model}/A_{tunnel}$. In the case of the facilities with open test sections, the ratio was defined as $\beta_{oj} = A_{model}/A_{jet}$, where A_{jet} is the area of the inflow stream.

Table 2. Summary of PIV experiments on TVs of wind turbines models.

Research laboratory	Wind Tunnel	TS $[m \times m]$	D $[m]$	β [%]	β_{oj} [%]	Tip shape
MEXICO [6, 7]	oj □	9.5×9.5^a	4.5	–	18	tapered
Middle East TU [14]	oj ○	2.27^a	0.94	–	31	flat
TU Delft [11, 12]	oj ⬡	2.85×2.85^a	2	–	39	flat
Iowa SU [26, 27]	cc □	2.4×2.3	0.25	1	–	flat
ENSAM [8]	cc □	1.35×1.65	0.5	9	–	flat
Current study	cc □	4.2×4.2	3	40	–	tapered

Wind tunnel - cc: closed test section, oj: open jet, and shape of the oj or the test section. TS: Test section width× height, (a) area of the oj section. D: diameter. β was rounded to the unit.

4. Results and discussion

In the interest of brevity, only part of the experimental and simulation cases are presented in this section, together with an overall analysis. For completeness, a set of results can be found in App. A.

4.1. Tip vortex core location

Figure 5 shows the Q-criterion contour normalized by its maximum value for the PIV measurements at a TV age of $\phi = 40°$. The dashed line represents the tip-line when the TV was shed ($\phi = 0°$). It can be seen that there is a zone with a maximum value surrounded by several local maximums (secondary peaks) with a considerable percentage magnitude.

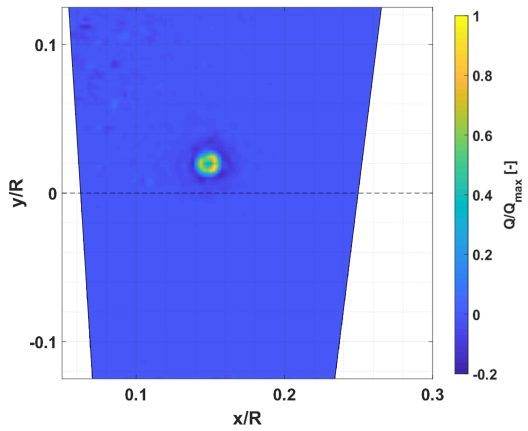

Figure 5. Normalized Q-criterion contour at TV age of $\phi = 40°$ of one set of images from BeRT PIV results

It is conceivable that this spreading of the Q-magnitude was caused by the tip shape. The shedding of the TV is not as clean and strong as in the case of flat tip shape, i.e. there is a continuous shedding associated with the aspect ratio of the tapered tip. Similar behavior was reported by Madsen et al. [28], where was shown a strong difference in the shedding and development of the TV with several tip shape types.

Figure 6 shows the location of the peaks of the Q-criterion for the experimental and simulated cases, at a TV age of $\phi = 40°$. In the case of the PIV measurements, all the recorded images are plotted together showing, as expected, that the maximum Q-value (i.e. the TV core location) was unstable due to the jittering, which also affects the secondary peaks.

The average location for this case is at $(x/R, y/R) = (0.152, 0.021)$ with a jittering radius of $r_j/R = 0.02$. This radius corresponds to 2% of the rotor radius and was smaller than in previous experiments [26, 27], where was shown a wandering zone between $6 - 30\%$R.

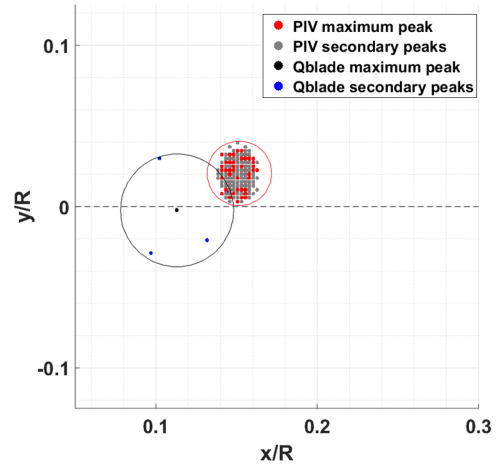

Figure 6. TVs location based on Q-criterion from PIV and QBlade simulation at TV age of $\phi = 40°$.

In the case of the far-field simulation from QBlade, the center of the TV was found more upstream and outboard the tip $(x/R, y/R) = (0.113, -0.003)$, compared to the experimental results. Here, the jittering was not expected. However the Q-criterion shows spreading of the magnitude, which results in a zone 75% larger than the PIV measurements. The latter was assumed as the result of the discretization of the tip in the simulations and is proposed to use additional panels in the tip for further comparisons. Nevertheless, the spreading zone radius increment still represents only the $3.5\%R$, therefore, a smaller value than the tapered tip zone and smaller than the jittering zone from similar experiments as mentioned above. The rest of the radii analysis cases is addressed in section 4.3 together with the estimation of the core radius.

The tracking of the TVs from the PIV measurements, QBlade simulation and similar experiments is presented in Fig. 7. It can readily be seen a consistent more downstream position in the current experiments compared to the simulations when the same TV age was taken into account.

Regarding the lateral movement towards the wall, the QBlade simulation exhibits a stronger expansion, moving outboard the tip line already at the TV age of 40°. In the case of the similar experiments, the movement of the TV outboard the tip is nearly after the rotor while the current experimental values remain inboard the tip even up to a TV age of 60° and a downstream distance of $x/R = 0.22$.

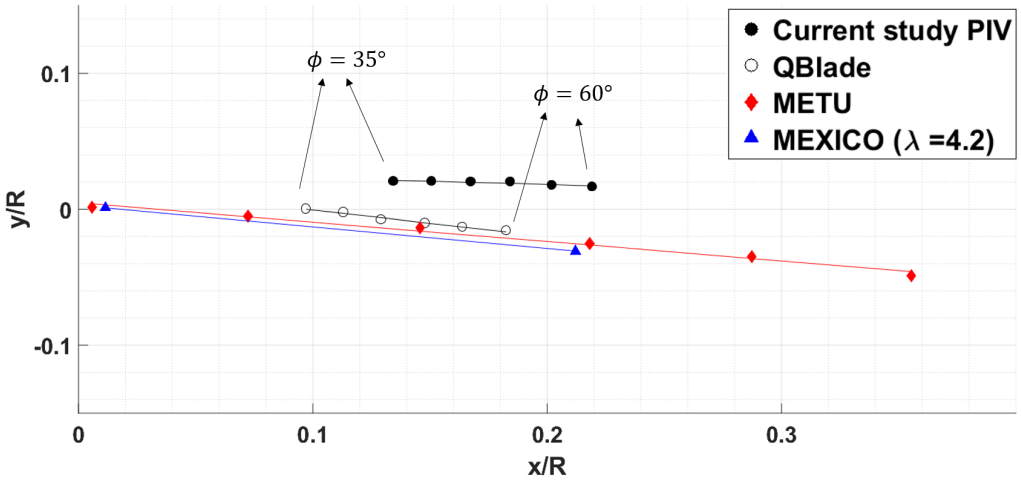

Figure 7. Average locations of the TVs based on Q-criterion from PIV measurements, QBlade simulation and similar PIV experiments [14, 7]. straight lines represent the linear fit of each experiment and simulation.

It is conceivable that the farther downstream convection can be explained by the delay in the wake expansion. The lateral position of the TV is more inboard than the simulations, which suggest a smaller radius of the TV helical wake. However, the axial distance of vortex cores is similar in the experiments and simulations, $\Delta x/R \approx 0.037$ (see Fig. 7), which suggests a similar axial velocity.

The fact the vortex cores are further downstream in the experiments indicates that the vortex followed a shorter path in the early stages of development. It is noted at this point that to confirm this hypothesis, early TV age data is needed.

4.2. Convection velocity

The location of the TVs was tracked in time to study their behavior and estimate the axial, u_c, and lateral, v_c, convection velocities.

The temporal evolution of the axial location of the TVs was found linear for both, experiments and simulation, which implies a constant axial convection velocity. Table 3 shows the ratio between axial convection velocity and freestream velocity, u_c/u_∞, together with the blockage ratio for the current study and similar experiments. It can be seen that there is no direct correlation between blockage and velocity ratios. At the same time the similar velocity ratio between the current PIV experiments and QBlade simulation, $\Delta u_c/u_\infty = 4.5\%$, suggests that there is no major influence of the level of blockage on the axial convection velocity of the TV.

Table 3. Axial convection velocity and blockage ratios for experiments and simulation.

Study	BeRT QBlade	Iowa SU	ENSAM	MEXICO	METU	TU Delft	BeRT PIV
β [%]	0	1	9	18	31	39	40
u_c/u_∞	0.89	0.90	0.78	0.92	0.79	0.73	0.85

Nevertheless, a large influence of the blockage over the lateral location is shown in Figures 8 and 9, regarding the current PIV measurements. An acceleration, caused by the walls ($y/R \leq 0$) and consequently, a negative thrust coefficient can be observed.

Figure 8 also provides evidence that the small difference in axial convection velocities between the current PIV experiments and QBlade simulations, $\Delta u_c/u_\infty$, is a consequence that the TV is still in the shadow of the rotor, in the case of the experiments.

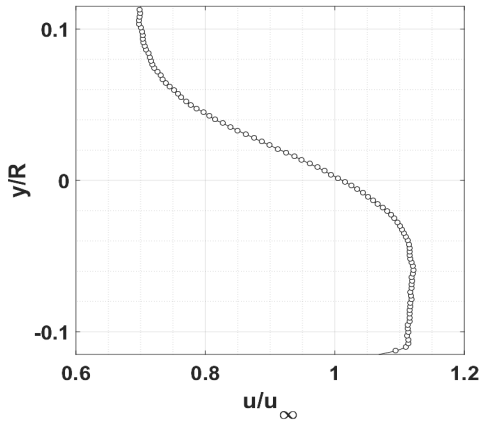

Figure 8. Normalized axial velocity distribution over the lateral direction at axial position $x/R = 0.22$ and TV age of $\phi = 40°$.

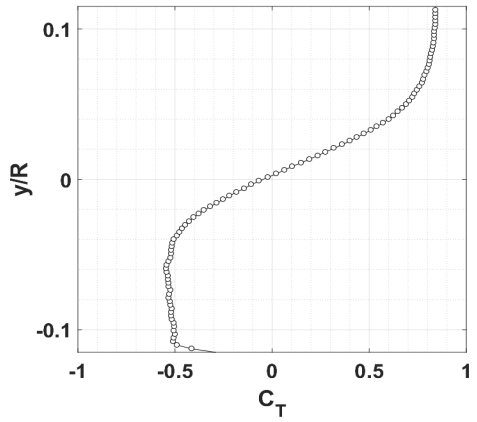

Figure 9. Thrust coefficient over the lateral direction at axial position $x/R = 0.22$ and TV age of $\phi = 40°$.

The lateral location of the TVs was modeled by means of a quadratic function. The known behavior of the lateral location of the TV can be summarized as inboard (concave shape) and outboard (convex) movement to the tip-line in agreement with the results [29, 7] and is depicted with the red line in Fig. 11.

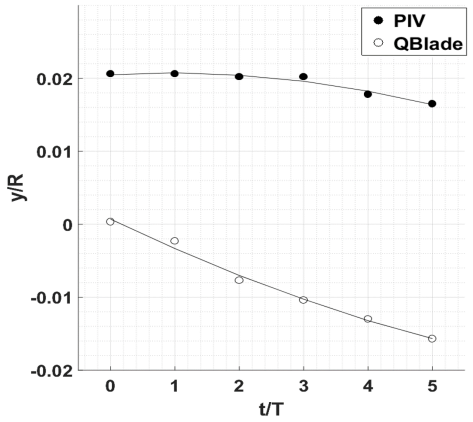

Figure 10. Temporal evolution of the lateral location of the TV from PIV measurements and QBlade simulation.

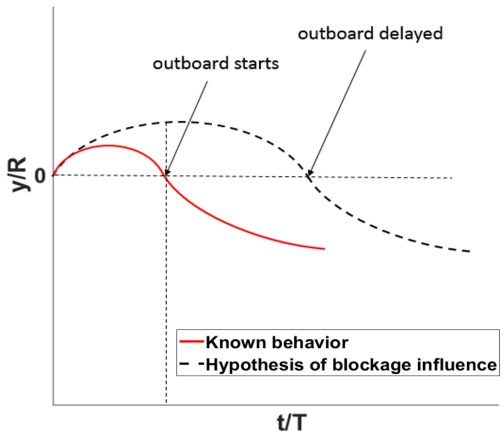

Figure 11. Temporal evolution of the lateral location of the TV and hypothesis of blockage influence.

In the current study, experiments and simulations have an opposite evolution, as shown in Fig. 10, where the PIV measurements exhibit a concave shape and QBlade a convex. One hypothesis of this behavior is that the blockage delays the outboard movement of the TV as is shown in Fig. 11 with the dashed line. It can be noticed that the trend of Fig. 10 fits in between the outboard starts and outboard delayed from Fig. 11, which supports this idea. Nevertheless, further measurements should be taken in order to confirm this behavior.

4.3. Core radius and Strength

The core radius of the TV was estimated from the swirl velocity, after the subtraction of the convection velocities in order to analyze only the vortex-induced velocity. For all the cases the TV core radius was found as $r_c/R = 0.012$, except by the TV age $\phi = 50°$ where the value was $r_c/R = 0.014$. An important remark for this is that the ratio between the TV radius of the core and jittering takes values in the range of $r_c/r_j = 0.5 - 0.8$, thus the wandering radius can go up more than the half of the TV core.

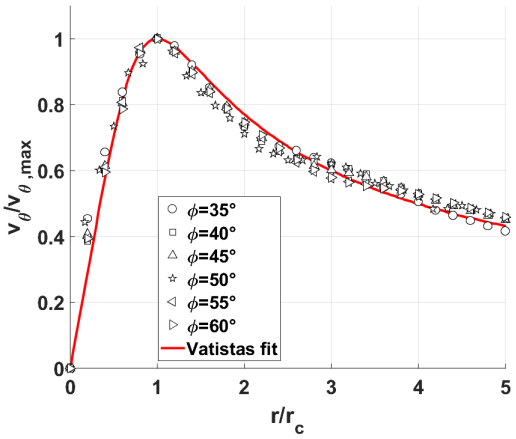

Figure 12. Swirl velocity distribution from the TV core center at different TV ages. In additon, fit of the turbulence model by Vatistas [7].

Figure 12 shows the normalized swirl velocity over the normalized radius for all the TV ages studied. Additionally, the TV turbulent model was plotted, with a turbulence parameter value of $\alpha = 0.65$. Similar values were found by Maalouf et al. [8] with a range of $\alpha = 0.55 - 0.7$ and Ostovan et al. [14] with a value of $\alpha = 0.7$. It was noted that although the experiments in these studies were performed in wind tunnels with significantly different turbulence levels $Ti = 6\%$, 0.5% [8] and 3% [14], the turbulence parameters values were very similar. Therefore, the freestream turbulence intensity is not the only factor to take into account in the turbulence parameter model.

The strength of the TV was determined based on the circulation, by integrating the vorticity field over one core radius surface from the TV core center, Γ_c, and four times the core radius, Γ_∞. The latter was made in order to avoid the dispersion of the vorticity due to the tip shape. In each case, the magnitudes of the circulation were similar for all the TV ages. Table 4 shows the circulation results with their standard deviation

Table 4. Circulation of the TV for the current measurements and simulation.

$\Gamma\ [m^2 s^{-1}]$	PIV	QBlade
Γ_c	1.15 ± 0.01	0.36 ± 0.03
Γ_∞	1.68 ± 0.01	1.75 ± 0.03

The large difference with respect to the core circulation is due to the spread of the vorticity shedding of the discretization panels at the tip in the case of the Qblade simulation. Nevertheless, once the integrated surface was extended, the circulation was similar with a difference up to 4%.

The Reynolds number based on the circulation in this case, it takes the value of $Re_\nu = \Gamma_\infty/\nu = 108k$. The latter can be classified as a fully turbulent vortex, based on [30], which agrees with the Vatistas turbulence parameter away from the laminar values $\alpha = 1$.

5. Conclusions

Phase-locked Stereo particle image velocimetry measurements in the near wake of a wind turbine model under the influence of wind tunnel walls with a large blockage were performed. Lift line free vortex wake simulations with the same wind turbine model geometry were calculated in the absence of the walls. The experimental results were compared to simulations and similar experiments according to the tip vortices characteristics, concluding as follow:

- The TV path is significantly influenced by blockage both in the axial and radial directions. In more detail, TVs travel farther downstream and more inboard compared to simulations and similar experiments with considerably less blockage.
- The magnitude contours of the invariant Q suggested an unsynchronized vortex shedding along the tapered tip zone.
- The axial convection velocity was found constant in each case. Similar results between current experiments and simulation were found $\Delta u_c = 4.5\% u_\infty$.
- In the present experiments and simulations, the TVs move outboard in agreement with published wind tunnel results for the same vortex age range.
- The turbulent vortex model fit the swirl velocity with a parameter of $\alpha = 0.65$, in agreement with the high circulation Reynolds number of $108k$.
- The ratio between the tip vortex core and jittering radius is in the range of $r_c/r_j = 0.5 - 0.8$.
- The strength of the tip vortex remained similar between the tip vortex age of $\phi = 35° - 60°$.

Acknowledgments

R. Soto-Valle would like to thank ANID PFCHA/Becas Chile-DAAD/2016 − 91645539

References

[1] Noura B, Dobrev I, Dizene R, Massouh F and Khelladi S 2012 *Proc. of the Institution of Mechanical Engineers, Part A: J. of Power and Energy* **226** 664–73
[2] Vermeer L 1994 *Proc. 5th European Wind Energy Association Conf. & Exhibition, Thessaloniki, Greece* pp 805–8
[3] Sørensen J N, Mikkelsen R, Sarmast S, Ivanell S and Henningson D 2014 *J. Phys.: Conf. Ser.* **524** 012155
[4] Vermeer L, Briaire J and van Doorne C 1995 *British Wind Energy Association Annual Wind Energy Conf. Warwick, UK* pp 59–64
[5] Vermeer L, van Bemmelen J and Over E 1996 *Proc. 10th IEA Symp. on Aerodynamics of Wind Turbines, Edinburgh, UK* pp 77–82
[6] Snel H, Schepers J and Montgomerie B 2007 *J. Phys.: Conf. Series* **75** 012014
[7] Snel H, Schepers G and Siccama N 2009 *47th AIAA Aerospace Sciences Meeting, Orlando, Florida, USA* p 1217
[8] Maalouf B, Dobrev I and Massouh F 2009 *19th Congr. Français de Mécanique, Courbevoie, France*
[9] Hu H, Yang Z and Sarkar P 2012 *Experiments in fluids* **52** 1277–94
[10] van der Wall B G and Richard H 2006 *Experiments in Fluids* **40** 798–812
[11] Micallef D, Akay B, Ferreira C S, Sant T and van Bussel G 2014 *J. Phys.: Conf. Ser.* **555** 012074
[12] Micallef D, Akay B, Sant T, Ferreira C S and van Bussel G 2011 *Proc. European Wind Energy Association Conf. & Exhibition, Brussels, Belgium*
[13] Micallef D, van Bussel G, Ferreira C S and Sant T 2013 *Wind Energy* **16** 529–44

[14] Ostovan Y, Akpolat M T and Uzol O 2019 *J. of Solar Energy Engineering* **141** 011006
[15] Grant I, Mo M, Pan X, Parkin P, Powell J, Reinecke H, Shuang K, Coton F and Lee D 2000 *J. of Wind Engineering and Industrial Aerodynamics* **85** 177–89
[16] Marten D, Wendler J, Pechlivanoglou G, Nayeri C N and Paschereit C 2013 *Int. J. of Emerging Technology and Advanced Engineering* **3** 264–69
[17] Vatistas G H 2006 *J. of Aircraft* **43** 1577–79
[18] Klein A C, Bartholomay S, Marten D, Lutz T, Pechlivanoglou G, Nayeri C N, Paschereit C O and Krämer E 2018 *Wind Energy Science* **3** 439–60
[19] Bartholomay S, Michos G, Perez-Becker S, Pechlivanoglou G, Nayeri C, Nikolaouk G and Paschereit C O 2018 *Proc. Wind Energy Symposium, American Institute of Aeronautics and Astronautics, Kissimee, Florida, USA*
[20] Pechlivanoglou G, Fischer J, Eisele O, Vey S, Nayeri C and Paschereit C 2015 *12th German Wind Energy Conf. (DEWEK), Bremen, Germany*
[21] Tangler J 2000 *Proc. American Wind Energy Association Wind Power, Palm Springs, California, USA* vol 500 (National Renewable Energy Laboratory) p 28410
[22] Hunt J, Wray A and Moin P 1988 *Proc. Summer Program Center for Turbulence Reserch, Stanford, California, USA* vol S88 (Center for Turbulence Research Report) pp 193–208
[23] van der Wall B and Richard H 2005 *Proc. 31st European Rotorcraft Forum, Florence, Italy*
[24] Marten D, Lennie M, Pechlivanoglou G, Nayeri C N and Paschereit C O 2016 *Journal of Engineering for Gas Turbines and Power* **138** 072601
[25] Marten D, Paschereit C O, Huang X, Meinke M H, Schroeder W, Mueller J and Oberleithner K 2019 *American Institute of Aeronautics and Astronautics Scitech 2019 Forum, San Diego, California, USA* p 2080
[26] Yang Z, Sarkar P and Hu H 2011 *Proc. 29th American Institute of Aeronautics and Astronautics Applied Aerodynamics Conf. Honolulu, Hawaii, USA* p 3815
[27] Yang Z, Sarkar P and Hu H 2012 *J. of visualization* **15** 39–44
[28] Madsen H and Fuglsang P 1996 RISO-R-891(EN) Tech. rep. Risoe National Laboratory
[29] Micallef D, Ferreira C S, Sant T and van Bussel G 2016 *Wind Energy* **19** 1485–501
[30] Ramasamy M and Leishman J G 2006 *J. of the American Helicopter Society* **51** 92–103

Appendix A

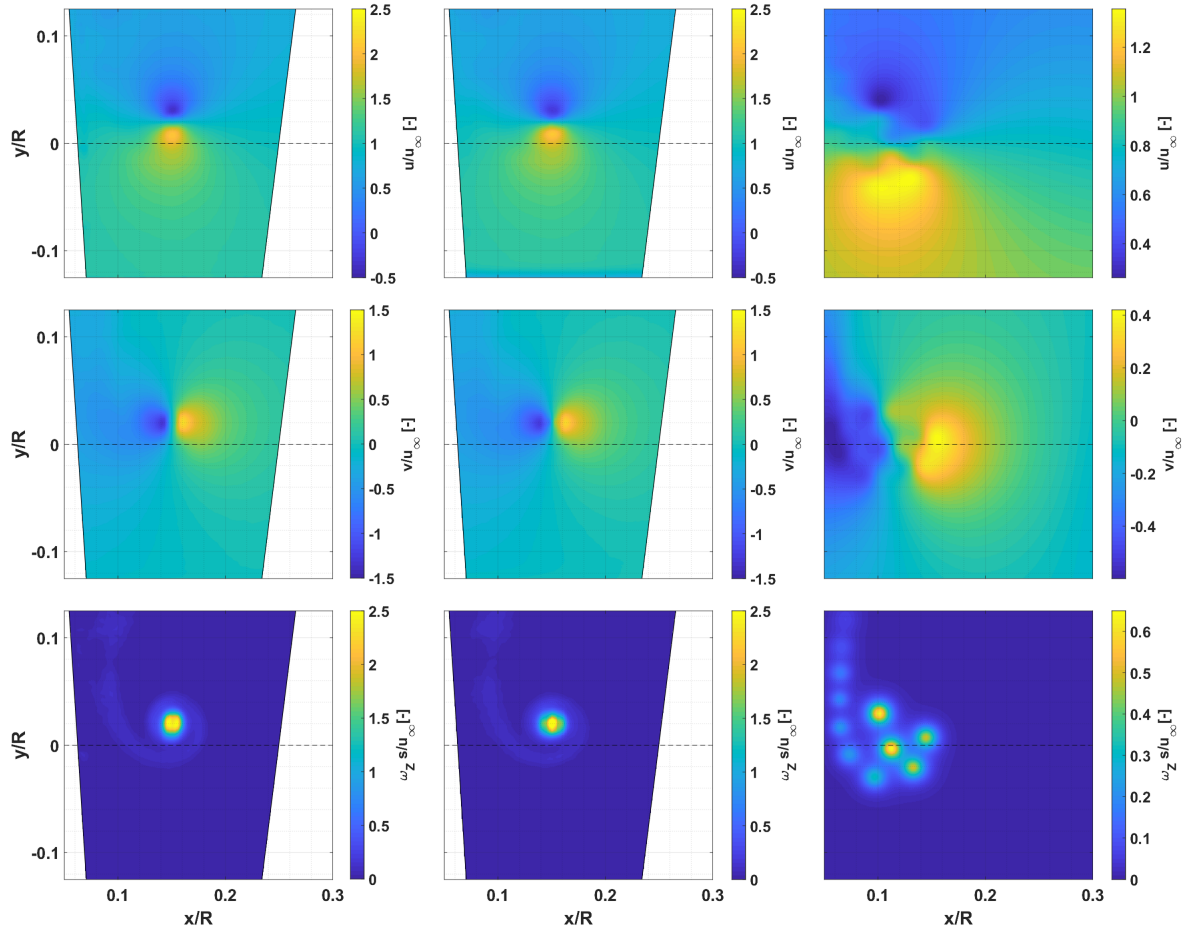

Figure A. Experimental and simulation results from BeRT at TV age of $\phi = 40°$. columns from left to right: normal average, conditional average, and QBlade simulation. The rows from top to bottom: normalized axial velocity, normalized lateral velocity, and normalized vorticity.